Appl. Magn. Reson. (2008) 35, 73–94
DOI 10.1007/s00723-008-0144-2
Printed in The Netherlands

Applied
Magnetic Resonance

ESEEM Measurements of Local Water Concentration in D_2O-Containing Spin-Labeled Systems

A. D. Milov[1], **R. I. Samoilova**[1], **A. A. Shubin**[2,3], **Yu. A. Grishin**[1], and **S. A. Dzuba**[1,3]

[1] Institute of Chemical Kinetics and Combustion, Russian Academy of Sciences, Novosibirsk, Russian Federation
[2] Boreskov Institute of Catalysis, Russian Academy of Sciences, Novosibirsk, Russian Federation
[3] Novosibirsk State University, Novosibirsk, Russian Federation

Received 18 January 2008

Abstract. To calibrate electron spin echo envelope modulation (ESEEM) amplitudes with respect to the deuterium water content in spin-labeled biological systems, ESEEM of nitroxide TEMPO has been studied in frozen glassy D_2O-dimethylsulfoxide mixtures of different composition. The interaction between the unpaired electron of nitroxide and the deuterium nuclei manifests itself in a cosine Fourier transform spectrum as the sum of a narrow line with the doublet quadrupole splitting and of a broad one. The narrow line arises from interaction with distant deuterium nuclei, the broad one arises from interaction with nearby nuclei belonging to nitroxide-water molecule complexes. The dependence on water concentration was found to be nonlinear for the intensity of the narrow line and close to linear for the intensity of the quadrupole doublet. Therefore, the intensity of the quadrupole doublet is suggested as a measure of concentration of free water around a spin label in biological objects. Fourier transform line shape was theoretically simulated for different model distributions of water molecules around the spin label. Simulations confirm the linear dependence of the quadrupole doublet intensity on water concentration seen in the experiment. The suggested approach was applied to analyze data for spin-labeled dipalmitoylphosphatidylcholine (DPPC) and DPPC-cholesterol D_2O-hydrated model membranes. The concentration of free water near the spin-labeled fourth carbon atom along the lipid chain was estimated as 5.2 and 7.2 M for DPPC and DPPC-cholesterol membranes, respectively.

1 Introduction

Penetration of water into membranes influences the membrane permeability and supramolecular structure of the embedded peptides and therefore the total functioning of biological cells. It was studied by different experimental and theoretical approaches [1–3]. Recently, a new approach [4–7] has been suggested which uses the advantage of the electron spin echo envelope modulation (ESEEM). ESEEM originates from anisotropic hyperfine interaction (HFI) with nearby nu-

clei [8, 9]. Comparison of ESEEM amplitude taken for lipids spin-labeled at different positions along the lipid chain allows studying the water penetration profile. In these works deuterated water D_2O was used to distinguish hydrogen atoms of water from those of lipid molecules and to increase the amplitude of ESEEM that is known to be much larger for deuterons at the X-band.

ESEEM induced by interaction of spin labels with surrounding water also has been used to elucidate the location of spin-labeled peptide embedded into the model phospholipid membrane [10]. This was done by comparing the ESEEM results with data on water penetration profile obtained in ref. 6.

However, for the lack of the quantitative calibration of ESEEM amplitude, in refs. 4–7 only the shape of the water penetration profile was studied. For more detailed information, quantitative data are desirable. It is the purpose of this paper to get the calibration of the ESEEM amplitude that would allow obtaining the local water (D_2O) concentration.

We use nitroxide 2,2,6,6-tetramethylpiperidine-1-oxyl (TEMPO) dissolved in glassy D_2O-dimethylsulfoxide (DMSO) mixture as a model system. This solvent allows varying water content in a wide range, simultaneously keeping the capability to form a low-temperature glass that is an important precondition for observation of the ESEEM phenomenon.

Nitroxides are known to form complexes with OH-containing molecules by hydrogen bonding between oxygen atoms of a nitroxide and hydrogen atom of an OH group [11–16]. The complexes may contain one or two ligand molecules. The formation of nitroxide complexes in solvents containing OH groups (methanol-toluene, ethanol-toluene, water-glycerol) has been studied using a two-pulsed ESE technique [8]. In the present work we use a three-pulsed stimulated ESEEM [8, 9] which provides more simple and resolved spectra at the frequency domain.

The suggested approach is additionally testified for solutions of nitroxides in methanol CH_3OD.

2 Experimental

2.1 ESEEM Experiment

Stimulated ESEEM was studied using a Bruker ESP380 Fourier transform (FT) electron spin resonance (ESR) spectrometer equipped with a homebuilt low-Q resonator suitable for measurements with a quartz Dewar filled with liquid nitrogen. A microwave pulse sequence $\pi/2-\tau-\pi/2-T-\pi/2$ with a pulse duration of 16 ns was used. The interval between the first and second pulses τ was equal to 200 ns in all measurements. The ESEEM was recorded by scanning the T delay starting from 80 ns, with a step of 16 ns, covering the range of 550 points. The unwanted echoes were eliminated using a Bruker PulseSpel Software, applying a four-step phase cycling program $+(0, 0, 0)$, $-(0, \pi, 0)$, $-(\pi, 0, 0)$, and $+(\pi, \pi, 0)$ [17]. The spectrometer magnetic field was set to the maximum of the nitroxide EPR spectrum.

2.2 Materials

As a spin probe we used a stable nitroxide TEMPO. DMSO (Sigma), D_2O and methanol CH_3OD (Isotop, St. Petersburg; deuterium content of 99%) were used without further purification. The concentration of D_2O in a D_2O-DMSO mixture was varied from 9.3 to 27.9 M. This concentration range was selected to provide a glassy state upon freezing to 77 K. In methanol solutions, 5% of ethanol was added to avoid crystallization. The TEMPO concentration was 10^{-2} M.

2.3 Simulations

Simulations were performed using a 12-processor computer cluster (12×2.53 MHz Pentium 4 CPU, PC Linux OS).

3 Results and Discussion

3.1 ESEEM of Nitroxide TEMPO in a D_2O-DMSO Mixture

ESEEM amplitude as a function of the delay T between the second and the third pulse, $V(T)$, was studied for glassy solutions of stable nitroxide TEMPO in D_2O-DMSO mixtures of different composition. From experimental $V(T)$ decays we obtained a normalized ESEEM decay [6], $V_n(T) = V(T)/\langle V(T)\rangle - 1$, where a smooth function $\langle V(T)\rangle$ was obtained by fitting the oscillating $\ln(V(T))$ experimental decays by a polynomial function. Figure 1 shows some examples of $V_n(T)$ time traces. One can see that these traces oscillate around zero. Data in Fig. 1 shows that the ESEEM depth depends on the D_2O concentration.

In our analysis we used the cosine FT:

$$F_C = \int_{t_1}^{t_2} V_n(t)\cos(2\pi ft)\mathrm{d}t\,, \tag{1}$$

where $t = \tau + T$ is taken in microseconds, $\tau = 0.2$ μs, f is frequency in megahertzs, the values $t_1 = 0.28$ μs and $t_2 = 9.064$ μs present the experimental range of t variations. Note that the form in which the variable t is taken here corresponds to the theoretical expressions known for stimulated ESEEM [8]. Fourier transformation Eq. (1) was performed numerically with a homebuilt computer program.

Note that the suggested data treatment results in spectral densities which have absolute values and may be used for comparison of different D_2O-containing systems.

Figure 2 shows spectral densities F_C obtained by applying Eq. (1) to experimental $V_n(T)$ time dependences shown in Fig. 1. Several features are seen in Fig. 2: a narrow line with a central frequency of 2.28 MHz and a half-height width

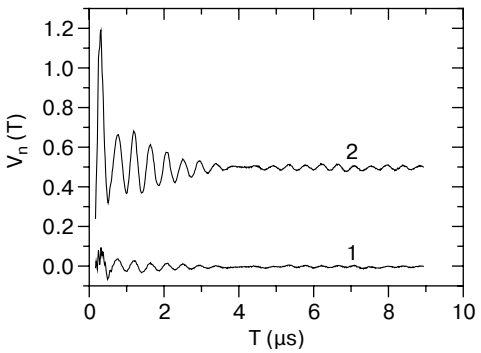

Fig. 1. Normalized stimulated ESEEM (see text) for TEMPO solutions in D_2O-DMSO mixture. The D_2O concentration is 9.3 and 26.4 M for curves 1 and 2, respectively. Curve 2 is shifted upwards by 0.5.

of about 0.26 MHz; this line is splitted into a doublet; and a broad line covering the range from 1.5 to 3.5 MHz with a half-height width of about 1 MHz.

According to the analysis performed in ref. 6, the narrow line is caused by weak interaction of the unpaired electron of nitroxide with distant deuterium nuclei. Doublet splitting is induced by weak nuclear quadrupole interaction of deuterium nuclei in water molecules. The broad line arises from strong interaction between the unpaired electron and deuterium nuclei in a water molecule coupled with nitroxide via hydrogen bonding.

The main goal of this work is to find suitable spectral parameters for estimating water concentration in the vicinity of spin labels. As possible candidates for these parameters we have chosen the intensities of the narrow A_N and broad A_B lines and the intensity of the quadrupole doublet Δ. Figure 2 depicts how these parameters are measured. Figure 3 presents the experimental dependences of the intensities of the narrow (A_N) and broad (A_B) lines for frozen glassy D_2O-DMSO

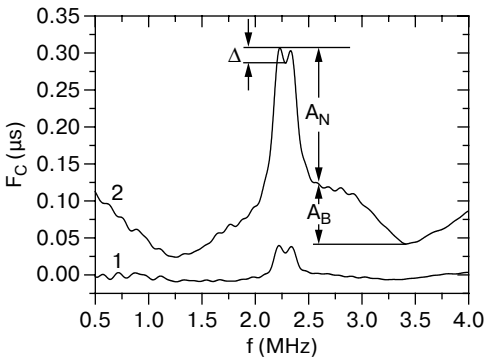

Fig. 2. Cosine FT of data shown in Fig. 1. Curve 2 is shifted upwards by 0.1. Three spectral parameters – intensity of the narrow line A_N, intensity of the broad line A_B, and intensity of the doublet splitting Δ – are shown.

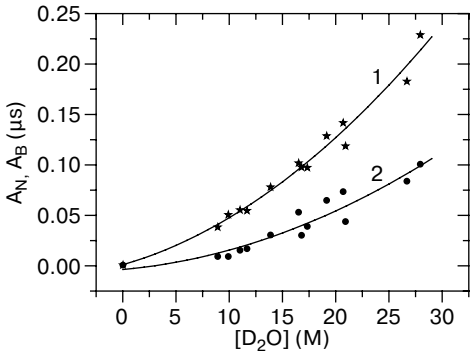

Fig. 3. Dependence of the intensities of the narrow (1) and broad (2) lines for TEMPO in a D_2O-DMSO mixture at 77 K (see Fig. 2). The points at zero concentration were obtained for a glassy H_2O-DMSO mixture. The curves are the second-order polynomial fits.

mixtures as a function of water concentration, [D_2O]. The curves drawn in Fig. 3 are the second-order polynomial fits.

The half-height widths of both narrow and broad lines were found to be independent on water concentration (data not given).

Figure 3 shows that intensities of the narrow and broad lines both increase with increasing [D_2O]. However, these dependences are not linear. For the broad line that is assigned to the interaction of spin labels with bound water [6], this nonlinearity may be readily explained by the formation of radical-water complexes whose concentration must depend on [D_2O]. As the narrow line is assigned to the interaction of spin labels with distant deuterons [6], which are expected to belong to free bulk water only, its intensity is expected to be proportional simply to [D_2O]. The nonlinear dependence of A_N on [D_2O] may be explained by the disturbance of the water molecules distribution in the close vicinity of the spin label because of formation of nitroxide-water complexes.

So, our experimental data show that the narrow line is not good enough to serve as a tool for the measurement of free D_2O concentration because it seems to depend on the formation of complexes. For different spin-labeled systems, both the constant of the complex formation and the structure of the complexes may differ, which will influence the relation between water concentration and the intensity of the narrow line.

The intensity of the quadrupole doublet denoted in Fig. 2 as Δ also depends on water concentration (see Fig. 4). As follows from Fig. 4, for water concentration below 20 M the Δ value dependence on [D_2O] may be described as a linear function

$$\Delta = d[D_2O]\,. \tag{2}$$

The empirical d value obtained from the slope of the straight line in Fig. 4 is $(1.0 \pm 0.12) \cdot 10^{-3}$ μs/M.

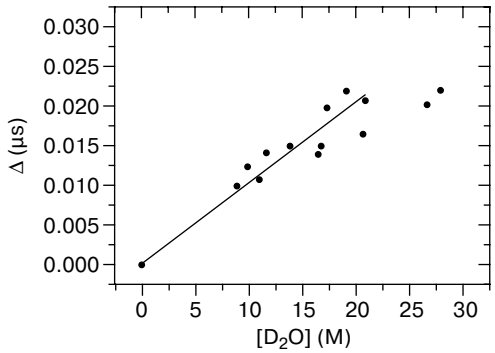

Fig. 4. Dependence of the intensity of the quadrupole doublet Δ (see Fig. 2) on water concentration. Straight line is drawn through the experimental points for concentrations below 20 M. The point at zero concentration was obtained for a glassy H_2O-DMSO mixture.

Therefore, for quantitative estimation of the free water concentration one may use the quadrupole doublet and the empirical Eq. (2) for its intensity. The reason why this intensity, different from that of the narrow line, is linearly dependent on water concentration will be analyzed below on the basis of the results of theoretical simulations.

3.2 Results of Theoretical Simulations

The method described in the Appendix was used to simulate cosine FT spectra of normalized ESEEM for various models of deuterium nuclei locations regarding the spin label. Figure 5 shows the results for a randomly oriented electron–deuteron pair, for different distances R in the pair. One can see that the spectral line in Fig. 5 is centered at the deuteron Larmor frequency. Its width is about 0.20 MHz for large distances R and increases with decreasing R. If R exceeds 0.5 nm, a doublet splitting is observed in the spectra. This splitting is ascribed to the deuteron quadrupole interaction. (According to our estimations, at 0.5 nm the magnitudes of HFI and nuclear quadrupole interaction [NQI] become comparable.) Both the line width and the doublet splitting resemble rather well the experimentally observed line shape for the narrow line (see Fig. 2).

Our simulations of ESEEM in nitroxide-water complexes with the geometrical parameters used in ref. 6 (data not given) reproduced rather well previously published data [6]. These simulations resulted in a broad line very close to that seen in Fig. 2.

The narrow line emerges in Fig. 5 at smaller distances as compared with the distances for which the quadrupole splitting appears. So, if water distribution in the nearest surrounding is disturbed because of formation of water-nitroxide complexes, this may manifest itself in the intensity of the narrow line but simultaneously may not influence the intensity of the quadrupole doublet, if these disturbances are located closer than 0.5 nm to the spin label.

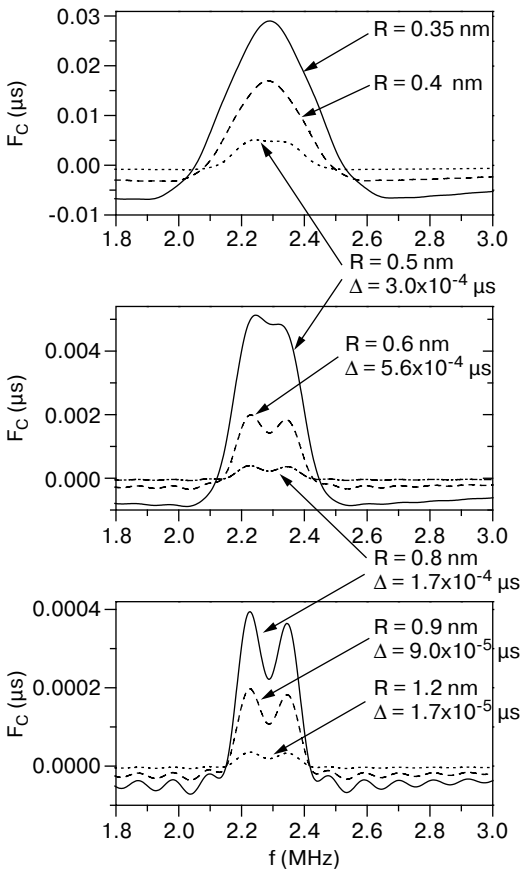

Fig. 5. Cosine FT (F_C) simulated for a model system consisting of one bulk water deuteron located at a distance R from the unpaired electron. The angle ψ between the symmetry axes of HFI and NQI tensors (see Appendix, Eq. (A30)) is averaged.

Figure 6 shows the calculated FT spectrum for the system in which bulk water is distributed uniformly outside a spherical cavity of radius R_{min}. The calculation is given for D_2O concentration of 26.4 M. As follows from Fig. 6, Δ depends substantially on the distance R_{min}. Similar dependences were found for other water concentrations (data not given).

Figure 7 shows the dependences of the normalized intensity of the quadrupole doublet, $d_{calc} = \Delta/[D_2O]$, as a function of $[D_2O]$, for various R_{min}. Figure 7 shows that d_{calc} is almost independent of water concentration for each given value of R_{min}, within the employed range of 0.35 nm < R_{min} < 1.5 nm. This result is in full agreement with the experimental observation presented by empirical Eq. (2).

Figure 8 demonstrates the parameter d_{calc} as a function of R_{min}. (As was shown in Fig. 7, this parameter is almost independent of water concentration.) The d_{calc} value reaches its maximum at R_{min} = 0.5 nm. As was already mentioned, at this distance the value of anisotropic HFI is close to the quadrupole split-

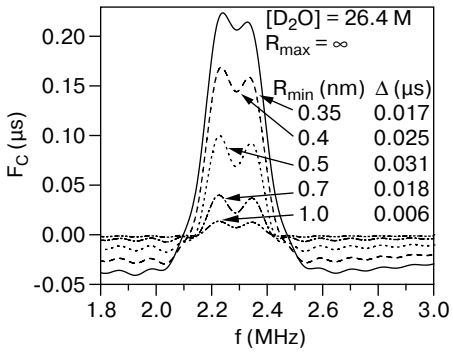

Fig. 6. Cosine FT (F_C) simulated for a model system consisting of an unpaired electron at the center of an empty spherical cavity of radius R_{min} surrounded by the molecules of bulk water with concentration $[D_2O]$ = 26.4 M.

ting value. When $R_{min} < 0.5$ nm, the anisotropic HFI smoothes the quadrupole splitting, and d decreases with decreasing R_{min}. For $R_{min} > 0.5$ nm, the d value decreases with increasing R_{min} due to the decrease of the electron–nuclear interaction.

The experimental value $d = 1.0 \cdot 10^{-3}$ μs/M (see above) corresponds to two possible distances R_{min}, 0.4 and 0.6 nm in Fig. 8. Note that the distance of 0.4 nm approximately corresponds to the radius of the second coordination sphere (see ref. 6 for the detailed geometry).

It is interesting to estimate for a given R_{min} the thickness of the water layer which makes the largest contribution to the quadrupole doublet amplitude Δ. To this end, we calculated the Δ values for the case when free water is enclosed between two spheres of radii R_{min} and R_{max}. The analysis performed indicates that

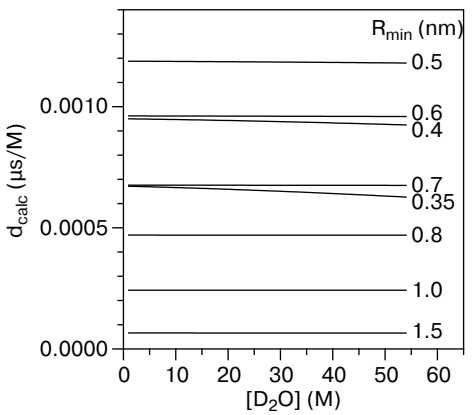

Fig. 7. Calculated d_{calc} value versus the concentration (see Eq. (2)) for the model presented in Fig. 6 for different radii R_{min} of a spherical cavity.

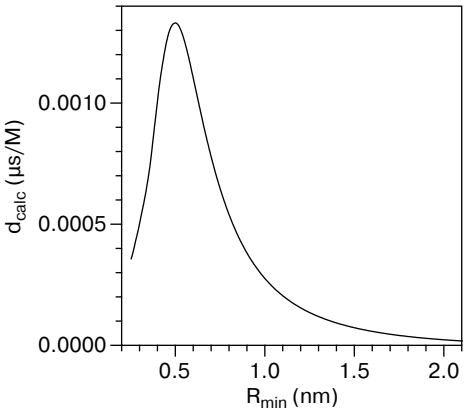

Fig. 8. Simulated dependence of the d_{calc} value (see Eq. (2)), averaged over free water concentration given in Fig. 7, as a function of the radius R_{min}.

for various values of R_{min} lying in the range from 0.4 to 0.7 nm the main contribution to the quadrupole doublet intensity (about 75%, data not given) arises from water molecules located at the distance $R < R_{max} = 1$ nm. This estimates the effective size of the spin probe for determining free water concentration.

3.3 TEMPO Solutions in CH_3OD

To additionally prove the suggested calibration, we applied it to another system of frozen glassy solutions of nitroxide TEMPO in methanol CH_3OD. Deuterium concentration in this system is 24.7 M. We obtained FT spectra (data not given) very similar to those shown in Fig. 2, with $\Delta = 0.01 \pm 0.0015$ μs. Assuming the validity of Eq. (2) for this system and taking into account that the number of deuterium nuclei in CH_3OD is twice less than that in D_2O, the deuterium concentration is estimated as 20 ± 5.4 M. This value is close to the actual one.

3.4 Water Concentration in Hydrated Model Lipid Membranes

Finally, we apply the suggested analysis for estimating water concentration in the nearest environment of spin labels in hydrated lipid model membranes. Figure 9 shows the cosine FT spectra for D_2O-hydrated dipalmitoylphosphatidylcholine (DPPC) model membranes with added lipids spin-labeled at fourth carbon position along the lipid tail, with and without cholesterol. These spectra were obtained from original ESEEM time traces (with fixed $\tau = 204$ ns) [6], kindly presented by D. A. Erilov (Institute of Chemical Kinetics and Combustion, Novosibirsk, Russia), which we treated exactly in the same way as described above. One can see that spectra shown in Fig. 9 are very similar to those presented in Fig. 2. The Δ values derived from Fig. 9 are $(5.2 \pm 1.0) \cdot 10^{-3}$ and $(7.2 \pm 1.4) \cdot 10^{-3}$ μs for spin-

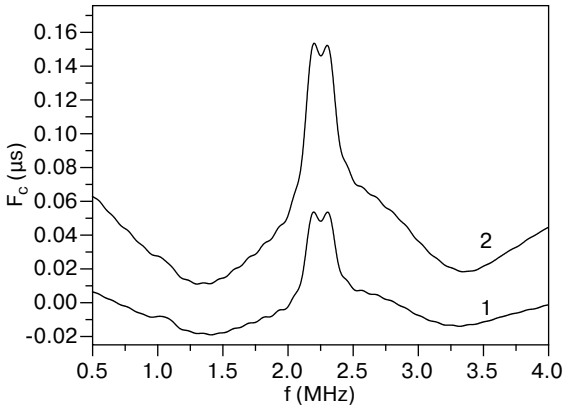

Fig. 9. Cosine FT of experimental ESEEM for spin-labeled D_2O-hydrated DPPC membranes (see Fig. 2). Curve 1, DPPC membranes; curve 2, DPPC-cholesterol (1:1 mol/mol) mixture membranes. Curve 2 is shifted upwards by 0.05.

labeled lipids in DPPC and DPPC-cholesterol model membranes, respectively. Water concentrations near the spin labels estimated from given experimental Δ values using Eq. (2) were found to be 5.2 ± 1.8 and 7.2 ± 2.4 M in DPPC and DPPC-cholesterol membranes, respectively.

As was indicated above, the interaction between a spin label and free bulk water deuterons spreads to 1 nm. It is known for the hydrated DPPC membranes that the distance from the fourth carbon atom to the water layer also is about 1 nm [18]. It makes necessary the analysis of the interaction between the spin label and free water located outside the model membrane, at its natural concentration of 55 M. By the method given in the Appendix, cosine FT ESEEM spectra were calculated for spin labels located at the distance R_{min} from the plane re-

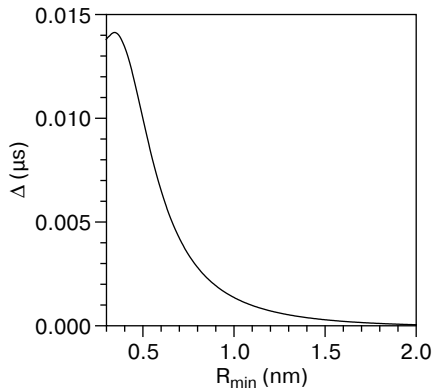

Fig. 10. Simulated dependence of the quadrupole doublet intensity Δ (Eq. (2)) as a function of distance R_{min} from D_2O-filled half-space ([D_2O], 55 M).

stricting the infinite half-space filled with water. Figure 10 shows dependence of the quadrupole doublet intensity Δ on the distance R_{min}. The curve in Fig. 10 indicates that at the distance of 1 nm the Δ value is about 10^{-3} μs/M, which is substantially lower than the aforementioned experimental values. This justifies neglecting the influence of water outside the model membrane in the present estimation of water concentration near the spin labels.

4 Conclusions

ESEEM in solutions of nitroxide TEMPO in frozen glassy D_2O-DMSO mixtures shows that cosine FT contains narrow and broad lines centered at the deuteron Zeeman frequency. Simulations show that the narrow line is produced by distant nuclei while the broad one by close nuclei from nitroxide-water complexes. The narrow line manifests a doublet splitting which is induced by NQI.

The experimentally found dependence of the narrow line intensity on water concentration is nonlinear, which may be explained by disturbance of the water molecules distribution in the close vicinity of the spin label because of formation of the nitroxide-water complex.

From the other side, experimental data show that the quadrupole doublet intensity is linearly proportional to free water concentration. This linear dependence is confirmed also by theoretical calculations. According to these calculations, quadrupole splitting arises at distances larger than those where the narrow line appears, therefore the mentioned disturbance at small distances here could be less important.

On the basis of this finding, a method for estimating water concentration near the spin label may be suggested which involves measuring the quadrupole doublet intensity and comparing it with the calibrated dependence obtained in this work for a D_2O-DMSO mixture. This method was additionally testified in this work for solutions of the spin label in methanol CH_3OD.

Using the obtained calibration, for the D_2O-hydrated model phospholipid membranes the concentration of free water around the spin-labeled fourth carbon atom along the lipid tail was estimated to be 5.2 and 7.2 M for DPPC and DPPC-cholesterol membranes, respectively.

It is shown in simulations that free water filling the intermembrane space does not influence ESEEM of spin labels located further than 1 nm from the membrane surface.

Appendix: Calculation of ESEEM Effects for Different Models of D_2O Distribution

A.1 General Consideration

Spin-echo signals were calculated assuming the full excitation of ESR spectrum by ideally nonselective microwave pulses. It has been known that stimulated

ESEEM due to the interaction with N nuclei can be presented in this case as [19, 20]

$$V(\tau,T)=\frac{1}{2}\mathrm{Re}\left(\prod_{i=1}^{N}\mathrm{Tr}\left(G_i^{\alpha}(\tau,T)\right)+\prod_{i=1}^{N}\mathrm{Tr}\left(G_i^{\beta}(\tau,T)\right)\right), \tag{A1}$$

where

$$G_i^{\alpha}(\tau,T)=\frac{1}{2I_i+1}\exp\left\{-\mathrm{i}\hat{J}_i^{\alpha}(\tau+T)\right\}\exp\left\{-\mathrm{i}\hat{J}_i^{\beta}\tau\right\}\exp\left\{\mathrm{i}\hat{J}_i^{\alpha}(\tau+T)\right\}\exp\left\{\mathrm{i}\hat{J}_i^{\beta}\tau\right\},$$

$$G_i^{\beta}(\tau,T)=\frac{1}{2I_i+1}\exp\left\{-\mathrm{i}\hat{J}_i^{\beta}(\tau+T)\right\}\exp\left\{-\mathrm{i}\hat{J}_i^{\alpha}\tau\right\}\exp\left\{\mathrm{i}\hat{J}_i^{\beta}(\tau+T)\right\}\exp\left\{\mathrm{i}\hat{J}_i^{\alpha}\tau\right\}, \tag{A2}$$

and operators $\hat{J}_i^{\alpha(\beta)}$ are given by

$$\hat{J}_i^{\alpha(\beta)}=-\omega_{I_i}\hat{I}_z^i\pm\frac{1}{2}\left(A_{zx}^i\hat{I}_x^i+A_{zy}^i\hat{I}_y^i+A_{zz}^i\hat{I}_z^i\right)+\mathscr{H}_Q^i. \tag{A3}$$

Here, A^i is the complete HFI tensor (isotropic and anisotropic components) and $\mathscr{H}_Q^i$ is the NQI Hamiltonian for the ith nucleus

$$\mathscr{H}_Q^i=\sum_{\mu,\nu=x,y,z}\hat{I}_{\mu}^i Q_{\mu\nu}^i\hat{I}_{\nu}^i. \tag{A4}$$

The approximation of the axially symmetric HFI and NQI tensors was used in all calculations performed in this work. In this case the HFI tensor is of the form

$$A_{\mu\nu}^i=A_{\perp}^i\delta_{\mu\nu}+\left(A_{\parallel}^i-A_{\perp}^i\right)\mathbf{n}_{\mu}^i\mathbf{n}_{\nu}^i,$$

where $\mathbf{n}^i$ is the unit vector along the axial direction of HFI tensor. In the dipole–dipole approximation this vector is directed from the unpaired electron to the ith nucleus, and the HFI tensor can be approximated as

$$A_{\mu\nu}^i=a_i\delta_{\mu\nu}+T_i\left(\delta_{\mu\nu}-3\mathbf{n}_{\mu}^i\mathbf{n}_{\nu}^i\right).$$

Here, a_i and T_i are the constants (in units of cyclic frequency, s^{-1}) of isotropic and dipole–dipole HFI, respectively:

$$T_i=-\frac{g_e\beta_e g_{I_i}\beta_N}{\hbar r_i^3}.$$

Thus, for the deuterium nucleus T_D (MHz) $= (2\pi)^{-1} \cdot 10^{-6} T_D$ (s^{-1}) $= -0.012136/r^3$, where r is the distance between the unpaired electron and the deuteron (in nanometers). Analogously, the axially symmetric NQI tensor (in units of cyclic frequency, s^{-1}) is given by

$$Q^i_{\mu\nu} = \frac{\pi C^i_Q}{2I_i(2I_i - 1)}\left(3\mathbf{u}^i_\mu \mathbf{u}^i_\nu - \delta_{\mu\nu}\right),$$

where $C^i_Q = C^i_Q$ (Hz) is the NQI constant for the ith nucleus, and the unit vector $\mathbf{u}^i$ defines the axial direction of the NQI tensor.

To perform calculations, it is convenient to detail Eq. (A2) for $G^{\alpha(\beta)}_i(\tau,T)$ and, e.g., $G^{\alpha}_i(\tau,T)$ can be represented as follows [19–21]:

$$G^{\alpha}_i(\tau,T) = \sum_{\substack{m,m',\\ m'',m'''}} B^{\alpha,i}_{mm'm''m'''} \exp\left(-i\varepsilon^{\alpha,i}_m t - i\varepsilon^{\beta,i}_{m'}\tau + i\varepsilon^{\alpha,i}_{m''}t + i\varepsilon^{\beta,i}_{m'''}\tau\right). \qquad \text{(A5)}$$

In this equation, $t = \tau + T$, and $\varepsilon^{\alpha(\beta),i}_m$ ($m = -I_i,...,I_i$) are the eigenvalues of operators $\hat{J}^{(\alpha)}_i$ and $\hat{J}^{(\beta)}_i$, respectively. The coefficients $B^{\alpha,i}_{mm'm''m'''}$ are given by the product of four overlap integrals $S^i_{mm'} = \langle m_{\alpha,i}|m'_{\beta,i}\rangle$ of eigenfunctions $|m_{\alpha,i}\rangle$ and $|m'_{\beta,i}\rangle$ of the operators $\hat{J}^{(\alpha)}_i$ and $\hat{J}^{(\beta)}_i$, respectively:

$$B^{\alpha,i}_{mm'm''m'''} = S^i_{mm'}(S^i_{m''m'})^* S^i_{m''m'''}(S^i_{mm'''})^*.$$

In a similar fashion, we have

$$G^{\beta}_i(\tau,T) = \sum_{\substack{m,m',\\ m'',m'''}} B^{\beta,i}_{mm'm''m'''} \exp\left(-i\varepsilon^{\beta,i}_m t - i\varepsilon^{\alpha,i}_{m'}\tau + i\varepsilon^{\beta,i}_{m''}t + i\varepsilon^{\alpha,i}_{m'''}\tau\right). \qquad \text{(A6)}$$

In this case the following condition is satisfied: $B^{\beta,i}_{mm'm''m'''} = B^{\alpha,i}_{m'm''m'''m}$. Equations (A5) and (A6) are convenient and quite sufficient for a single calculation of the ESE signal. However, they contain a fourfold sum with respect to m, m', m'' and m'''. That is why, due to cumbersome calculations, their use is ineffective for averaging of the stimulated echo signal simultaneously over all possible orientations of the paramagnetic center, spatial distribution of nuclei and probably over other parameters of the model. Nevertheless, in the case of stimulated echo signal the use of the symmetry of coefficients $B^{\alpha(\beta),i}_{mm'm''m'''}$ with respect to both the rearrangement of indices and complex conjugation allows us to reduce the fourfold sum in Eqs. (A5) and (A6) to the twofold one. This method, similar to that used in ref. 22, allows us to accelerate ESEEM calculations almost 100 times even for the spin $I = 1$ of deuteron.

For further analysis, let us divide all N deuterons into two groups: $N = 2k + N_b$. The first group includes $2k$ deuterons ($k = 0, 1, 2$) of k water molecules bound with the complex with nitroxide. The second group contains N_b deuterons of bulk

(matrix) water molecules for which both their distance and the orientation of their NQI tensors are randomly distributed relative to the complex of nitroxide with k molecules of bound water. Of particular interest is the limiting case: $N_b \to \infty$, which will be considered here for two models. In the first model the complex of the nitroxide with k molecules of bound water is spherically symmetric, surrounded by bulk water deuterons and is located (relative to the unpaired electron) at the center of an empty spherical cavity of radius R_{min}. The system contains the complexes with random orientations relative to the external magnetic field B which is parallel to the z-axis of the laboratory system of coordinates. The concentration $[D_2O]$ of the surrounding water (and as a result, the concentration C_D of deuterons $C_D = 2[D_2O]$) beyond the cavity may vary. In the second model the position of the nitroxide complex with k water molecules is fixed relative to the infinitely thick D_2O layer approximated by the D_2O-filled half-space so that the effective distance from the unpaired electron to the half-space surface is also equal to R_{min}. The orientation of the entire system (the complex plus the D_2O-filled half-space) is considered as random with respect to the magnetic field B.

To obtain the spin-echo signal for the models under study, we should perform the integration over three Euler angles that define current orientation of the complex. In addition, for each current orientation of the complex it is necessary to perform averaging over three random spatial coordinates of each bulk water deuteron and three angular coordinates that define the orientation of NQI tensor of this deuteron with respect to the complex. However, it readily follows from Eqs. (A1)–(A4) that in the case of the full excitation of the ESR spectrum, ESEEM is independent of the rotation of the entire system as a whole through an arbitrary angle γ about the direction of the external magnetic field B (z-axis of the laboratory system of coordinates). Moreover, ESEEM due to HFI with N nuclei (in the presence of NQI, if $I_i \geq 1$) will not change if both HFI and NQI tensors of one of these nuclei (e.g., i) are rotated simultaneously through an arbitrary angle γ_i about the B direction. Indeed, $\mathrm{Tr}(G_i^{\alpha(\beta)}(\tau,T))$ in Eq. (A1) are independent of the arbitrary unitary transformation $\hat{M}$, i.e.,

$$\mathrm{Tr}\left(G_i^{\alpha(\beta)}(\tau,T)\right) = \mathrm{Tr}\left(\hat{M}G_i^{\alpha(\beta)}(\tau,T)\hat{M}^{-1}\right).$$

The independence of the ESE signal of angle γ_i can be verified quite readily if we choose operator $\hat{M}$ as

$$\hat{M} = \exp\left(-i\gamma_i \hat{I}_z^i\right),$$

and take into account that [23]

$$\hat{M}\hat{I}_\nu^i\hat{M}^{-1} = \sum_{\mu=x,y,z} m_{\mu\nu}\hat{I}_\mu^i .$$

Here, m is the orthogonal ($m^{-1} = \tilde{m}$), real 3×3 matrix corresponding to the rotation of a vector on the angle γ_i about the z-axis.

The independence of the ESE signal of the rotation of the spin system as a whole about the B direction allows us to perform the averaging only over two Euler angles, θ and φ (Fig. 11), that define orientation of the spin system (first rotation on the angle θ about the y-axis of the laboratory coordinate system and the second rotation on the angle φ about the new direction z'). Assuming that deuterons in coordinated water have fixed positions relative to the nitroxide, and that the spatial distribution of bulk water deuterons and their NQI tensors orientations are random, we have the following expression for the stimulated ESE signal:

$$V^{(k)}(\tau,T) = \frac{1}{2}\mathrm{Re}\left(\overline{\prod_{i=1}^{2k} \mathrm{Tr}\left(G_i^{\alpha}(\tau,T)\right)\left(\overline{\mathrm{Tr}(g^{\alpha}(\tau,T))}\right)^{N_b}} + \overline{\prod_{i=1}^{2k} \mathrm{Tr}\left(G_i^{\beta}(\tau,T)\right)\left(\overline{\mathrm{Tr}(g^{\beta}(\tau,T))}\right)^{N_b}} \right), \tag{A7}$$

where $\mathrm{Tr}(G_i^{\alpha(\beta)}(\tau,T))$ and $\mathrm{Tr}(g^{\alpha(\beta)}(\tau,T))$ are the contributions to the stimulated ESE signal from the deuterons of bound and bulk water molecule, respectively. The single line atop in the Eq. (A7) means the averaging over the angles θ and φ defining the orientation of entire system, i.e.,

$$\overline{X} = \int_0^{\pi} \mathrm{d}\theta \frac{\sin\theta}{2} \int_0^{2\pi} \frac{\mathrm{d}\varphi}{2\pi} X(\theta,\varphi)\,.$$

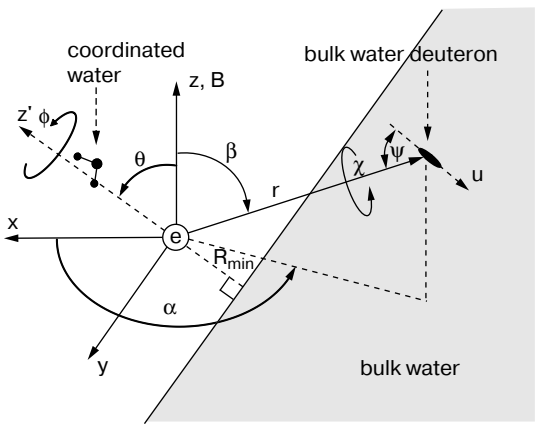

Fig. 11. Geometrical model used in simulations shown in Fig. 10. The axially symmetric NQI tensor of free water deuteron is shown as an ellipsoid and vector **u** shows the axial direction of this tensor. The y-axis of the laboratory coordinate system is chosen here parallel to the surface of bulk water. See text for details.

The double line atop in Eq. (A7) means the averaging of the contributions to the stimulated ESEEM originating from the interaction between the unpaired electron of the complex and one of the N_b deuterons of bulk water. This averaging is performed over both the possible orientation (relative to the complex) of deuteron NQI tensor and all admissible spatial locations of this deuteron. In Eq. (A7) it is taken into account that $\overline{\overline{\mathrm{Tr}(g^{\alpha(\beta)}(\tau,T))}}$ values depend on the orientation of the spin system as a whole, i.e., they can be functions of the angles θ and φ. However, it is clear from the symmetry of the system that in the model of spherically symmetric distribution of bulk deuterons about the nitroxide, $\overline{\overline{\mathrm{Tr}(g^{\alpha(\beta)}(\tau,T))}}$ are independent on θ and φ, while in the model of infinitely thick D_2O layer (D_2O-filled half-space) they depend only on the angle θ (Fig. 11). A further simplification of the problem is due to the fact that the deuteron NQI tensor used here is axially symmetric with the symmetry axis directed along the OD bond. Thus, the averaging over all possible relative orientations of the NQI tensor can be performed over only two angles, χ and ψ (Fig. 11). Moreover, it follows from the symmetry of the system that the range of ψ angle variation can be reduced by a factor of two: $0 \le \psi \le \pi/2$. It is convenient to perform the averaging over all admissible spatial deuteron locations r in spherical coordinates (r, β, α) shown in Fig. 11. In terms of the aforementioned assertion $\mathrm{Tr}(g^{\alpha(\beta)}(\tau,T))$ is independent of the azimuth angle α, while the range of the admissible range for this angle is determined by both the model of bulk D_2O distribution and current (θ and φ angles) orientation of the system as a whole. Therefore, in some symmetric cases the integration over the angle α can be performed analytically.

In the general case we have

$$\overline{\overline{\mathrm{Tr}\left(g^{\alpha(\beta)}(\tau,T)\right)}} = \int_V \mathrm{d}\nu \frac{c(\mathbf{r},\theta,\varphi)}{N_b} \left\langle \mathrm{Tr}\left(g^{\alpha(\beta)}(\tau,T)\right)\right\rangle_{\chi\psi}. \qquad \text{(A8)}$$

Here, V is the system volume, $\mathrm{d}\nu = r^2 \sin\beta \mathrm{d}r\mathrm{d}\beta\mathrm{d}\alpha$, $c(\mathbf{r},\theta,\varphi)$ is the current (i.e., depending on θ and φ) concentration of bulk water deuterons, so that

$$N_b = \int_V c(\mathbf{r},\theta,\varphi)\mathrm{d}\nu .$$

The partial double averages $\langle \mathrm{Tr} g^{\alpha(\beta)}(\tau,T)\rangle_{\chi\psi}$ in Eq. (A8) depend on r and β. They are defined as

$$\left\langle \mathrm{Tr}\left(g^{\alpha(\beta)}(\tau,T)\right)\right\rangle_{\chi\psi} = \int_0^{\pi/2} \mathrm{d}\psi \sin\psi \int_0^{2\pi} \frac{\mathrm{d}\chi}{2\pi} \mathrm{Tr}\left(g^{\alpha(\beta)}(\tau,T)\right). \qquad \text{(A9)}$$

Since $\lim_{r\to\infty} \left\langle \mathrm{Tr}\left(g^{\alpha(\beta)}(\tau,T)\right)\right\rangle_{\chi\psi} = 1$, and the volume integral

$$\int_V \left(1 - \left\langle \mathrm{Tr}\left(g^{\alpha(\beta)}(\tau,T)\right)\right\rangle_{\chi\psi}\right)\mathrm{d}\nu$$

has the finite limit at $V \to \infty$ (i.e., at $N_b \to \infty$, too), it follows from Eq. (A8) that

$$\lim_{N_b \to \infty} \left(\overline{\overline{\mathrm{Tr}\left(g^{\alpha(\beta)}(\tau,T) \right)}} \right)^{N_b} = \exp\left\{ -\int_V \mathrm{d}\nu c(\mathbf{r},\theta,\varphi) \left(1 - \left\langle \mathrm{Tr}\left(g^{\alpha(\beta)}(\tau,T) \right) \right\rangle_{\chi\psi} \right) \right\}. \quad \text{(A10)}$$

It is worth noting that due to the factor $c(\mathbf{r},\theta,\varphi)$ the limit in Eq. (A10) depends, in general, on the angles θ and φ. Using Eq. (A10) we have from Eq. (A7) in the limiting case of $N_b \to \infty$ a general formula for calculation

$$V^{(k)}(\tau,T) = \frac{1}{2}\mathrm{Re}\left(\overline{\prod_{i=1}^{2k} \mathrm{Tr}\left(G_i^{\alpha}(\tau,T) \right) \exp\left\{ -\int_V \mathrm{d}\nu c(\mathbf{r},\theta,\varphi) \left(1 - \left\langle \mathrm{Tr}\left(g^{\alpha}(\tau,T) \right) \right\rangle_{\chi\psi} \right) \right\}} \right.$$

$$\left. + \overline{\prod_{i=1}^{2k} \mathrm{Tr}\left(G_i^{\beta}(\tau,T) \right) \exp\left\{ -\int_V \mathrm{d}\nu c(\mathbf{r},\theta,\varphi) \left(1 - \left\langle \mathrm{Tr}\left(g^{\beta}(\tau,T) \right) \right\rangle_{\chi\psi} \right) \right\}} \right). \quad \text{(A11)}$$

A.2 Calculations for Concrete Models

For the model of spherically symmetric distribution of D_2O molecules around the nitroxide, we have

$$c(\mathbf{r},\theta,\varphi) = c(r) = \begin{cases} C_D, \text{ if } r \geq R_{\min}; \\ 0, \text{ else.} \end{cases} \quad \text{(A12)}$$

For the model of a thick layer (half-space) filled with D_2O, for the geometry shown in Fig. 11 the following relation holds

$$c(\mathbf{r},\theta,\varphi) = c(r,\alpha,\beta,\theta) = \begin{cases} C_D, \text{ if } \mathrm{sgn}(\cos\theta)\cos\beta \leq -\dfrac{R_{\min}}{r|\cos\theta|} - \sin\beta\cos\alpha|\tan\theta|; \\ 0, \text{ else.} \end{cases} \quad \text{(A13)}$$

With Eq. (A12), for the spherically symmetric model of D_2O distribution the integral over the angle α is easily calculated

$$\int_0^{2\pi} c(r)\mathrm{d}\alpha = \begin{cases} 2\pi C_D, \text{ if } r \geq R_{\min}; \\ 0, \text{ else.} \end{cases} \quad \text{(A14)}$$

With Eq. (A13), for the model of D_2O-filled half-space (Fig. 11) calculations result in

$$\int_0^{2\pi} c(\mathbf{r},\theta)\mathrm{d}\alpha = \begin{cases} 2\pi C_{\mathrm{D}} W(\theta,r,\beta), \text{ if } r \geq R_{\min}; \\ 0, \text{ else.} \end{cases} \tag{A15}$$

Here, for $\theta \neq 0, \pi/2, \pi$,

$$W(\theta,r,\beta) = \begin{cases} 0, \text{ if } \operatorname{sgn}(\cos\theta)\cos\beta > -\dfrac{R_{\min}}{r|\cos\theta|} + \sin\beta|\tan\theta|; \\ \dfrac{1}{\pi}\arccos\left(\dfrac{R_{\min}}{r\sin\beta\sin\theta} + \cot\beta\cot\theta\right), \text{ if} \\ \quad -\dfrac{R_{\min}}{r|\cos\theta|} - \sin\beta|\tan\theta| \leq \operatorname{sgn}(\cos\theta)\cos\beta \leq -\dfrac{R_{\min}}{r|\cos\theta|} + \sin\beta|\tan\theta|; \\ 1, \text{ if } \operatorname{sgn}(\cos\theta)\cos\beta < -\dfrac{R_{\min}}{r|\cos\theta|} - \sin\beta|\tan\theta|; \end{cases} \tag{A16}$$

and for $\theta = 0$ or $\theta = \pi$,

$$W\left(\begin{Bmatrix} 0 \\ \pi \end{Bmatrix}, r, \beta\right) = \begin{cases} 0, \text{ if } \operatorname{sgn}(\cos\theta)\cos\beta > -\dfrac{R_{\min}}{r}; \\ 1, \text{ if } \operatorname{sgn}(\cos\theta)\cos\beta \leq -\dfrac{R_{\min}}{r}; \end{cases} \tag{A17}$$

whereas for $\theta = \pi/2$,

$$W\left(\frac{\pi}{2}, r, \beta\right) = \begin{cases} 0, \text{ if } \sin\beta < \dfrac{R_{\min}}{r}; \\ \dfrac{1}{\pi}\arccos\left(\dfrac{R_{\min}}{r\sin\beta}\right), \text{ if } \sin\beta \geq \dfrac{R_{\min}}{r}. \end{cases} \tag{A18}$$

Substituting Eqs. (A12) and (A14) into Eq. (A11) we obtain that for the spherically symmetric distribution of D_2O the following expression is valid

$$V^{(k)}(\tau,T) = \frac{1}{2}\mathrm{Re}\left(\overline{\prod_{i=1}^{2k}\mathrm{Tr}\left(G_i^{\alpha}(\tau,T)\right)}\exp\left\{-4\pi C_{\mathrm{D}}\int_{R_{\min}}^{\infty}\mathrm{d}r\, r^2\left(1-\left\langle\mathrm{Tr}\left(g^{\alpha}(\tau,T)\right)\right\rangle_{\chi\psi\beta}\right)\right\}\right.$$
$$\left. + \overline{\prod_{i=1}^{2k}\mathrm{Tr}\left(G_i^{\beta}(\tau,T)\right)}\exp\left\{-4\pi C_{\mathrm{D}}\int_{R_{\min}}^{\infty}\mathrm{d}r\, r^2\left(1-\left\langle\mathrm{Tr}\left(g^{\beta}(\tau,T)\right)\right\rangle_{\chi\psi\beta}\right)\right\}\right), \tag{A19}$$

where the partial triple averages $\langle \mathrm{Tr}(g^{\alpha(\beta)}(\tau,T))\rangle_{\chi\psi\beta}$ depend on r, but are independent of the angles θ and φ

$$\left\langle \mathrm{Tr}\left(g^{\alpha(\beta)}(\tau,T)\right)\right\rangle_{\chi\psi\beta} = \int_0^{\pi} \mathrm{d}\beta \frac{\sin\beta}{2} \left\langle \mathrm{Tr}\left(g^{\alpha(\beta)}(\tau,T)\right)\right\rangle_{\chi\psi}.$$

Note that $\langle \mathrm{Tr}(g^{\alpha(\beta)}(\tau,T))\rangle_{\chi\psi\beta}$ can be considered as an averaged contribution from one deuteron located at a fixed distance r from the paramagnetic center. This contribution is averaged over all feasible orientations of deuteron with respect to the paramagnetic center and is additionally averaged over the random relative orientation of the axial HFI and NQI tensors of this deuteron. It follows from Eq. (A19), that in the case of the spherically symmetric distribution of bulk D_2O the contributions to the stimulated ESEEM from the deuterons of coordinated and bulk water molecules are uncorrelated.

Similarly, in the case of the model where D_2O occupies a half-space, the substitution of Eq. (A15) into Eq. (A11) gives

$$V^{(k)}(\tau,T) = \frac{1}{2}\mathrm{Re}\left(\int_0^{\pi} \mathrm{d}\theta \frac{\sin\theta}{2} \exp\left\{-2\pi C_{\mathrm{D}} \left\langle D^{\alpha}(\tau,T)\right\rangle_{\chi\psi\beta r}\right\} \int_0^{2\pi} \frac{\mathrm{d}\varphi}{2\pi} \prod_{i=1}^{2k} \mathrm{Tr}\left(G_i^{\alpha}(\tau,T)\right) \right.$$

$$\left. + \int_0^{\pi} \mathrm{d}\theta \frac{\sin\theta}{2} \exp\left\{-2\pi C_{\mathrm{D}} \left\langle D^{\beta}(\tau,T)\right\rangle_{\chi\psi\beta r}\right\} \int_0^{2\pi} \frac{\mathrm{d}\varphi}{2\pi} \prod_{i=1}^{2k} \mathrm{Tr}\left(G_i^{\beta}(\tau,T)\right) \right). \quad \text{(A20)}$$

Here, the fourfold integrals $\langle D^{\alpha(\beta)}(\tau,T)\rangle_{\chi\psi\beta r}$ depend on the angle θ and have the form

$$\left\langle D^{\alpha(\beta)}(\tau,T)\right\rangle_{\chi\psi\beta r} = \int_{R_{\min}}^{\infty} \mathrm{d}r\, r^2 \int_0^{\pi} \mathrm{d}\beta \sin\beta W(\theta,r,\beta) \left(1 - \left\langle \mathrm{Tr}\left(g^{\alpha(\beta)}(\tau,T)\right)\right\rangle_{\chi\psi}\right), \quad \text{(A21)}$$

whereas the factor $W(\theta,r,\beta)$ in this formula is given by Eqs. (A16)–(A18).

Equations (A19) and (A20) are presented here in the form used for numerical calculations. Note that in the general case $\mathrm{Tr}(G_i^{\alpha(\beta)}(\tau,T))$ and $\mathrm{Tr}(g^{\alpha(\beta)}(\tau,T))$ are the complex values. However, their imaginary parts are very small. It is known [19, 20] that in the absence of NQI, $\mathrm{Tr}(G_i^{\alpha(\beta)}(\tau,T))$ are the real values of $V_i^{\alpha(\beta)}(\tau,T)$. Thus, the nonzero imaginary parts arise only from NQI. Our model numerical calculations performed for the different spin values $1 \le I \le 9/2$ (data not given) indicate that the imaginary part of $\mathrm{Tr}(G_i^{\alpha(\beta)}(\tau,T))$ is less than 10^{-5}–10^{-3} of that of the real part. Moreover, the partial double averages $\langle \mathrm{Tr}(g^{\alpha(\beta)}(\tau,T))\rangle_{\chi\psi}$, calculated from Eq. (A9), were found to be exactly real. In addition, according to numerical simulation, for the arbitrary symmetric (not necessarily axial) HFI and NQI tensors the value of $\mathrm{Im}\{\mathrm{Tr}(G_i^{\alpha(\beta)}(\tau,T))\}$ averaged over two Euler angles (θ and φ) is also zero.

As for the contribution of spatially correlated deuterons of the coordinated water molecules, the interfering term $\mathrm{Im}\{\mathrm{Tr}(G_i^{\alpha(\beta)}(\tau,T))\}$ from various nuclei provides very small (of the order of 10^{-6}–10^{-4}) relative contribution to the spin-echo signal. Therefore, the general Eq. (A11) for $V_k(\tau,T)$ can be rewritten as

$$V^{(k)}(\tau,T)=\frac{1}{2}\left[\overline{\mathrm{Re}\left(\prod_{i=1}^{2k}\mathrm{Tr}\left(G_i^{\alpha}(\tau,T)\right)\right)\exp\left\{-\int_V \mathrm{d}\nu c(\mathbf{r},\theta,\varphi)\left(1-\left\langle \nu^{\alpha}(\tau,T)\right\rangle_{\chi\psi}\right)\right\}}\right.$$

$$\left.+\overline{\mathrm{Re}\left(\prod_{i=1}^{2k}\mathrm{Tr}\left(G_i^{\beta}(\tau,T)\right)\right)\exp\left\{-\int_V \mathrm{d}\nu c(\mathbf{r},\theta,\varphi)\left(1-\left\langle \nu^{\beta}(\tau,T)\right\rangle_{\chi\psi}\right)\right\}}\right],$$

or, as it follows from the above consideration, represented in the approximate (but practically exact) form

$$V^{(k)}(\tau,T)\approx\frac{1}{2}\left(\overline{\prod_{i=1}^{2k}V_i^{\alpha}(\tau,T)\exp\left\{-\int_V \mathrm{d}\nu c(\mathbf{r},\theta,\varphi)\left(1-\left\langle \nu^{\alpha}(\tau,T)\right\rangle_{\chi\psi}\right)\right\}}\right.$$

$$\left.+\overline{\prod_{i=1}^{2k}V_i^{\beta}(\tau,T)\exp\left\{-\int_V \mathrm{d}\nu c(\mathbf{r},\theta,\varphi)\left(1-\left\langle \nu^{\beta}(\tau,T)\right\rangle_{\chi\psi}\right)\right\}}\right),$$

where

$$V_i^{\alpha(\beta)}(\tau,T)=\mathrm{Re}\left\{\mathrm{Tr}\left(G_i^{\alpha(\beta)}(\tau,T)\right)\right\},$$

$$\nu^{\alpha(\beta)}(\tau,T)=\mathrm{Re}\left\{\mathrm{Tr}\left(g^{\alpha(\beta)}(\tau,T)\right)\right\}.$$

Note that the stimulation of quadrupole effects in the $\mathrm{Tr}(g^{\alpha(\beta)}(\tau,T))$ contributions from the distant bulk water deuterons can be also performed using approximate formulas derived in ref. 21, which are valid in the first order of the perturbation theory.

A.3 Numerical Stimulations

As was mentioned above, we use the approximation of the axial symmetry of the NQI tensor. The NQI constant C_Q for both the coordinated and bulk water deuterons was chosen to be equal to 215 kHz. The concentration $C(\mathbf{r})$ of the deuterons of bulk water surrounding the complex was approximated by Eqs. (A12) and (A13) for the model of spherically symmetric distribution of D_2O molecules around the nitroxide and for the model of the D_2O-filled half-space, respectively.

The value R_{min} of the minimum distance from the unpaired electron of the complex to the bulk D_2O deuterons was varied and served as the parameter of the model. When the upper limit R_{max} in numerical integration over r was infinite, it was limited by $R_{max} = 3$ nm. The eigenvalues and the eigenfunctions of operators $\hat{J}_i^{\alpha(\beta)}$ were determined using the program ZHEEV from the library of linear algebra programs LAPACK [24]. The final program code indicated a fairly fast performance. Therefore, the integration over various sets of Euler angles (θ, ϕ, β, χ, ψ) did not involve the available special procedures of powder averaging [25–27]. The integration over all variables was performed using the Simpson method. The number of integration intervals was chosen equal to 400–600 for $0 \le \theta \le \pi$, 100–200 for $0 \le \varphi \le 2\pi$, 100 for $0 \le \chi \le 2\pi$, 90 for $0 \le \psi \le \pi/2$, and 400 for $0 \le \beta \le \pi$. The integration over r was also performed by the Simpson method with a step of 0.005 nm. For direct comparison with experimental data (see Sect. 2) most of the parameters were chosen to be equal to the experimental ones. The $V^{(k)}(\tau,T)$ values were calculated for $\tau = 0.2$ μs at 550 points T_i (from $T_{min} = 0.08$ μs to $T_{max} = 8.864$ μs with a step of 0.016 μs). Finally, the time T average $\langle V^{(k)}(\tau,T)\rangle_T$ was calculated and the cosine FT of the normalized stimulated ESE signal

$$V_n^{(k)}(\tau,T) = \frac{V^{(k)}(\tau,T)}{\left\langle V^{(k)}(\tau,T)\right\rangle_T} - 1$$

over the variable $t = \tau + T$ ($0.28 \le t \le 9.064$ μs) was performed.

Initially (for a fixed τ) the arrays of integrals $\langle \mathrm{Tr}(g^{\alpha(\beta)}(\tau,T))\rangle_{\chi\psi\beta}$ (for various r and T) and $\langle \mathrm{Tr}(g^{\alpha(\beta)}(\tau,T))\rangle_{\chi\psi}$ (for various r, β, and T) were calculated and permanently stored in the computer memory. This stage was the most time consuming and required 1–1.5 days of continuous work of the computer cluster. It should be mentioned that in calculations of $\langle \mathrm{Tr}(g^{\alpha(\beta)}(\tau,T))\rangle_{\chi\psi}$ integrals the range of the β angles can be reduced to $0 \le \beta \le \pi/2$ because the values of these integrals are the same for β and $\pi-\beta$. In the course of subsequent calculations, all these integrals were read from the permanent computer memory and used in calculations with Eq. (A19) or with Eqs. (A20) and (A21), respectively.

Acknowledgments

We are grateful to Yuri Tsvetkov for useful discussion. This work was supported by the Russian Foundation for Basic Research (grants 06-03-89400-NWO and 060448021), and by Grant for Scientific Schools (nr. 62712006.3).

References

1. Aman, K., Lindahl, E., Edholm, O., Hakansson, P., Westlund, P.-O.: Biophys. J. **84**, 102–115 (2003)
2. Fitter, J., Lechner, R.E., Dencher, N.A.: J. Phys. Chem. B **103**, 8036–8050 (1999)
3. Bhide, S.Y, Berkowitz, M.L.: J. Chem. Phys. **123**, 224702 (2005)

4. Noethig-Laslo, V., Cevc, P., Arcon, D., Sentjurc, M.: Appl. Magn. Reson. **27**, 303–309 (2004)
5. Bartucci, R., Guzzi, R., Marsh, D., Sportelli, L.: Biophys. J. **84**, 1025–1030 (2003)
6. Erilov, D.A., Bartucci, R., Guzzi, R., Shubin, A.A., Maryasov, A.G., Marsh, D., Dzuba, S.A., Sportelli, L.: J. Phys. Chem. B **109**, 12003–12013 (2005)
7. Bartucci, R., Erilov, D.A., Guzzi, R., Sportelli, L., Dzuba, S.A., Marsh, D.: Chem. Phys. Lipids **141**, 142–157 (2006)
8. Dikanov, S.A., Tsvetkov, Yu.D.: Electron Spin Echo Envelope Modulation (ESEEM) Spectroscopy. CRC Press, Boca Raton, Fla. (1992)
9. Schweiger, A., Jeschke, G.: Principles of Pulse Electron Paramagnetic Resonance. Oxford University Press, Oxford (2001)
10. Salnikov, E.S., Erilov, D.A., Milov, A.D., Tsvetkov, Yu.D., Peggion, C., Formaggio, F., Toniolo, C., Raap, J., Dzuba, S.A.: Biophys. J. **91**, 1532–1540 (2006)
11. Dikanov, S.A., Tsvetkov, Yu.D.: J. Struct. Chem. **20**, 699–708 (1979)
12. Dikanov, S.A., Tsvetkov, Yu.D.: J. Struct. Chem. **20**, 800–802 (1979)
13. Dikanov, S.A., Astashkin, V.A., Tsvetkov, Yu.D.: J. Struct. Chem. **23**, 333–345 (1982)
14. Symons, M.C.R., Pena-Nuñez, A.: J. Chem. Soc. Faraday Trans. 1 **1985**, 2421–2435 (1985)
15. Improta, R., Scalmani, G., Barone, V.: Chem. Phys. Lett. **336**, 349–356 (2001)
16. Engstrom, M., Owenius, R., Vahtras, O.: Chem. Phys. Lett. **338**, 407–413 (2001)
17. Fauth, J.-M., Schweiger, A., Braunschweiler, L., Forrer, J., Ernst, R.R.: J. Magn. Reson. **66**, 74–85 (1986)
18. Nagle, J.F., Tristram-Nagle, S.: Biochim. Biophys. Acta **1469**, 159–195 (2000)
19. Mims, W.B.: Phys. Rev. B **5**, 2409–2419 (1972)
20. Dikanov, S.A., Shubin, A.A., Parmon, V.N.: J. Magn. Reson. **42**, 474–487 (1981)
21. Shubin, A.A., Dikanov, S.A.: J. Magn. Reson. **52**, 1–12 (1983)
22. Madi, Z.L., Van Doorslaer, S., Schweiger, A.: J. Magn. Reson. **154**, 181–191 (2002)
23. Rose, M.E.: Elementary Theory of Angular Momentum. Dover, New York (1995)
24. Linear Algebra PACKage: http://netlib.org/lapack/index.html
25. Ponti, A.: J. Magn. Reson. **138**, 288–297 (1999)
26. Eden, M.: Concepts Magn. Reson. A **18**, 24–55 (2003)
27. Stevensson, B., Eden, M.: J. Magn. Reson. **181**, 162–176 (2006)

Authors' address: Sergei Dzuba, Institute of Chemical Kinetics and Combustion, Russian Academy of Sciences, Institutskaya 3, 630090 Novosibirsk, Russian Federation
E-mail: dzuba@ns.kinetics.nsc.ru